WP15ER-PR(18) 20964

L Colas et al.

Perfectly Matched Layers for time-harmonic electromagnetic wave propagation in curved gyrotropic media

Preprint of Paper to be submitted for publication in
Journal of Computational Physics

This work has been carried out within the framework of the EUROfusion Consortium and has received funding from the Euratom research and training programme 2014-2018 under grant agreement No 633053. The views and opinions expressed herein do not necessarily reflect those of the European Commission.

Perfectly Matched Layers for time-harmonic electromagnetic wave propagation in curved gyrotropic media

L. Colas[1], J. Jacquot[2], J. Hillairet[1], W. Helou[1], W. Tierens[2], S. Heuraux[3], E. Faudot[3], L. Lu[1†], G. Urbanczyk[1]

[1]CEA, IRFM, F-13108 Saint Paul Lez Durance, France.
[2]Max-Planck-Institut für Plasmaphysik, Garching, Germany.
[3]Université de Lorraine - CNRS Institut Jean Lamour F-54011 Nancy.
† present address: TianQin Research Center for Gravitational Physics, School of Physics and Astronomy, Sun Yat-Sen University, Zhuhai 519082, P. R. China

Abstract:

This paper generalizes a Perfectly Matched Layer (PML) technique for emulating radiation at infinity in finite difference or finite element simulations of time-harmonic electromagnetic wave propagation in complex media. Extending a previous work in Cartesian coordinates [Jacquot2013], we formulate a PML as an artificial inhomogeneous lossy medium, following the stretching into the complex plane of a general system of three orthogonal curvilinear coordinates. The particular cases of cylindrical and toroidal geometries illustrate the general method. As a test problem to assess the new formulation in gyrotropic media, we analytically quantify the reflection of cylindrical waves by a radial PML in cylindrical geometry. The obtained reflection coefficient involves wave, PML and geometric parameters at the PML location. The new coefficient generalizes the one obtained earlier with Cartesian coordinates, and becomes equivalent when the effects of the local cylindrical curvature at the PML (stretched) location can be neglected. These curvature effects are outlined and the limitations they impose on the properties of the PML are quantified as a function of the relevant parameters. Finite element calculations of the test problem in two-dimensional cylindrical geometry are exploited to verify these properties numerically.

I. Introduction

This paper deals with the numerical simulation of time-harmonic electromagnetic (EM) wave propagation. In such problems the time-harmonic Maxwell's equations in the medium are complemented with suitable boundary conditions. In finite difference or finite element calculations of EM wave propagation, Perfectly Matched Layers (PMLs) aim at emulating radiation at infinity inside a bounded simulation domain. In complex media such as cold magnetized plasmas, featuring a gyrotropic dielectric tensor, gyrotropy introduces two different wave propagation eigenmodes, referred to as Fast and Slow waves in the context of plasma physics [Swanson2003]. In the literature PMLs were already devised for the propagation of one eigenmode of gyrotropic media, generally in two dimensions (2D) transverse to the direction of anisotropy, and described by a scalar Helmholtz equation [Velasco2009]. This result was recently extended in 3D for the two eigenmodes, described by a vectorial time-harmonic wave equation [Gondarenko2004] [Jacquot2013]. Reference [Bécache2017] explored the transient EM pulse propagation in uniaxial media using the Finite Difference Time Domain (FDTD) method and PMLs adapted for each eigenmode. Reference [Jacquot2013] implemented PMLs adapted for cold magnetized plasmas at the edge of (flattened) toric magnetic fusion devices in the Radio-Frequency (RF) module of the COMSOL finite element solver [COMSOL]. In this latter paper, PMLs were defined as artificial inhomogeneous lossy dielectric and magnetic media, where the standard equations of electrodynamics could be applied. This was achieved by stretching the conventional Cartesian coordinates of a flattened tokamak along prescribed trajectories in the complex plane.

For many realistic applications however, using Cartesian coordinates appears to be a limitation. Flattening a toric tokamak is an approximation, historically intended to enable using spectral methods of EM wave simulation. The limits of this approxipation have been explored both by modelling [Louche2011] [Jacquot2015] [Milanesio2017] and experiments in several frequency ranges [Bilato2004], [Ekedahl2015]. Cartesian PMLs can sometimes be kept in a curved geometry if the plasma-PML boundary remains flat. This is however not always possible, and in practice it might be inefficient: in uniaxial media for example, reference [Bécache2017] showed it necessary to stretch space along directions either parallel or perpendicular to the anisotropy. Otherwise propagative forward and backward waves might coexist, one of which cannot be damped by the PML. In view of simulating cylindrical RF plasma discharges (*e.g.* Capacively coupled discharges [Faudot2015], helicon discharges [Crombé2015], [Furno2017], ion cyclotron-heated ones [Crombé2015], [Gekelman2016]), toroidal devices (tokamaks [Jacquot2015]) or even more complex geometries (stellarators) in a more realistic way, it is therefore tempting to stretch the spatial coordinates along the principal directions defined by the device geometry. However, over such change, the differential operators **rot**(.) and div(.) appearing in Maxwell's equations modify their forms, due to the local curvature of the new coordinate systems [Angot1972]. This calls for re-formulating the PML.

One can also anticipate that curvature effects might modify the wave-reflection properties of the PML. A standard assessment of these PML properties in Cartesian geometry is to quantify the reflection of propagative or evanescent plane waves in homogeneous media as a function of the relevant simulation parameters. This was done extensively in [Jacquot2013] for plane waves in gyrotropic media. Criteria of low reflection could be established for tuning the PML parameters. Limitations were also outlined when propagative forward and backward waves coexist in the PMLs. While plane waves are well suited for PML benchmark in Cartesian geometry, they are generally not adapted in curved coordinates, and alternative test-problems should be looked for. Literature on these subjects is scarce, even for simple isotropic media.

The present paper proposes to generalize in curved coordinates the methodology applied in [Jacquot2013] for Cartesian coordinates. Firstly a PML is formulated as an artificial medium, following the stretching of a general system of three orthogonal curvilinear coordinates. Cylindrical and toroidal coordinates illustrate the general method. Secondly, in the particular case of cylindrical geometry, we further try to assess the PML properties: analytical criteria are defined for low reflection of waves by radial PMLs. We use for this purpose cylindrical waves that play in cylindrical geometry an equivalent role as plane waves in Cartesian coordinates. Cylindrical waves of gyrotropic media are recalled when the direction of anisotropy is along the axis of the cylinder. The PML reflection criteria involve wave, PML and geometric parameters at the PML location. The new results generalize those obtained earlier, and become equivalent when the effects of the local cylindrical curvature at the PML (stretched) location can be neglected. Curvature effects are outlined and the limitations they impose on the properties of the PML are quantified as a function of the relevant parameters. Finally, finite element calculations of the test problem in 2D cylindrical geometry are exploited to quantify these properties numerically.

II. PML formulation in curved coordinates as an artificial lossy dielectric medium

Throughout this paper we consider time-harmonic EM fields oscillating in time as $\exp(+i\omega_0 t)$ at pulsation ω_0. In the 3-dimensional (3D) Euclidian space, the EM fields **E** and **H** evolve according to Maxwell's equations in the frequency domain

$$\begin{cases} \mathbf{rotE} = -i\omega_0 B \\ \mathbf{rotH} = +i\omega_0 D + j_{\mathbf{ant}} \\ \operatorname{div} D = \rho_{ant} \\ \operatorname{div} B = 0 \end{cases} \qquad \text{(II.1)}$$

In equations (II.1) the oscillating current $\mathbf{j}_{\mathbf{ant}}$ imposed on the antenna structures, as well as the oscillating antenna space charge ρ_{ant}, were isolated from the self-consistent response of the medium to (**E**,**H**), incorporated in the linear local constitutive relations

$$\mathbf{D}=\boldsymbol{\varepsilon}(\omega_0)\mathbf{E} \; ; \; \mathbf{B}=\boldsymbol{\mu}(\omega_0)\mathbf{H}. \qquad \text{(II.2)}$$

Tensors $\boldsymbol{\varepsilon}(\omega_0)$ and $\boldsymbol{\mu}(\omega_0)$ can take very general forms. In references [Sachs1995], [Gedney1996], [Texeira1998], stretching the usual Cartesian coordinates into the complex plane was found beneficial to emulate radiating boundary conditions in a PML for problem (II.1). Besides, a formal analogy was outlined between the obtained PMLs matched to isotropic media and an artificial medium with modified dielectric and magnetic properties. In [Gondarenko2004], [Jacquot2013] the analogy was extended to more complex media with full dielectric permittivity $\boldsymbol{\varepsilon}$ and/or magnetic permeability $\boldsymbol{\mu}$ tensors, *e.g.* cold magnetized plasmas [Swanson2003]. In this section we would like to extend the technique to formulate PMLs by stretching the three principal directions defined by a system of three curved coordinates [Angot1972]. So far the generalization appears tractable only for orthogonal sets and stretching procedures that preserve this orthogonality.

A. Solving Maxwell's equations in stretched orthogonal curvilinear coordinates

In the 3D Euclidian space, we consider an orthogonal set of three curvilinear coordinates (u,v,w) such that $\nabla u.\nabla v=\nabla v.\nabla w=\nabla w.\nabla u=0$ everywhere. The system is characterized locally by the elementary distance ds defined as:

$$ds^2 = h_u^2(u,v,w)\,du^2 + h_v^2(u,v,w)\,dv^2 + h_w^2(u,v,w)\,dw^2 \qquad \text{(II.3)}$$

In this system we envisage a vector field $\mathbf{V}(u,v,w)$, whose components along the three orthogonal principal directions are $V_u(u,v,w)$, $V_v(u,v,w)$ $V_w(u,v,w)$. The differential operators div(.) and **rot**(.) appearing in Maxwell's equations (II.1) are then defined as [Angot1972]

$$\mathrm{div}(V) = \frac{1}{h_u h_v h_w}\left[\partial_u(h_v h_w V_u) + \partial_v(h_w h_u V_v) + \partial_w(h_u h_v V_w)\right] \qquad \text{(II.4)}$$

$$\mathbf{rot}(V) = \begin{bmatrix} \left[\partial_v(h_w V_w) - \partial_w(h_v V_v)\right]/h_v h_w \\ \left[\partial_w(h_u V_u) - \partial_u(h_w V_w)\right]/h_w h_u \\ \left[\partial_u(h_v V_v) - \partial_v(h_w V_w)\right]/h_u h_v \end{bmatrix} \begin{matrix} \cdot u \\ \cdot v \\ \cdot w \end{matrix} \qquad \text{(II.5)}$$

In the PML the spatial coordinates (u,v,w) are artificially stretched according to the rules $u \to t_u(u) = u_0 + \int_{u_0}^{u} S_u(t)\,dt$, $v \to t_v(v) = v_0 + \int_{v_0}^{v} S_v(t)\,dt$, $w \to t_w(w) = w_0 + \int_{w_0}^{w} S_w(t)\,dt$. The triplet (u_0, v_0, w_0) as well as the stretching functions $(S_u(u), S_v(v), S_w(w))$ are arbitrary and can be chosen conveniently for the required application. In particular, the stretching can be extended to the complex plane. The main difference with Cartesian geometry is the directions along which space is stretched. As for Cartesian frames it is essential that $S_u(u)$ depends only on u, $S_v(v)$ on v and $S_w(w)$ on w. Each coordinate is stretched "perpendicular to the other ones": the stretched coordinate system remains orthogonal and a relation similar to (II.3) applies, with $du = dt_u(u)/S_u(u)$ and metric elements evaluated at stretched location, such as $h_u(t_u(u),t_v(v),t_w(w)) = h_{tu}(u,v,w)$. If the stretching extends to the complex plane, h_{tu}, h_{tv} and h_{tw} might become complex, whereas they should be real positive before the stretching. Stretching functions are equal to 1 in the main simulation domain, where the properties of the original medium are preserved. In the PML, on the contrary, we request that the new local EM fields ($\mathbf{E}_{\mathbf{PML}}$, $\mathbf{H}_{\mathbf{PML}}$) at location (u,v,w) be the solutions (**E, H**) of the original wave problem (II.1) evaluated at stretched location $(t_u(u), t_v(v), t_w(w))$. To this end, problem (II.1) is replaced with a modified one

$$\begin{cases} \mathbf{rot}_s\left(E_{\mathbf{PML}}(u,v,w)\right) = -i\omega_0 \boldsymbol{\mu}\mathbf{H}_{\mathbf{PML}}(u,v,w) \\ \mathbf{rot}_s\left(H_{\mathbf{PML}}\right) = i\omega_0 \boldsymbol{\varepsilon}\mathbf{E}_{\mathbf{PML}} + j_{\mathbf{ant}} \\ \mathrm{div}_s\left[\boldsymbol{\varepsilon}\mathbf{E}_{\mathbf{PML}}\right] = \rho_{ant} \\ \mathrm{div}_s\left[\boldsymbol{\mu}\mathbf{H}_{\mathbf{PML}}\right] = 0 \end{cases} \qquad \text{(II.6)}$$

where $\mathbf{rot}_s(.)$ and $\mathrm{div}_s(.)$ denote the differential operators (II.4) and (II.5) with respect to the stretched curved coordinates. The modified differential operators $\mathbf{rot}_s(.)$ and $\mathrm{div}_s(.)$ are obtained from formulae (II.4) and (II.5) upon the substitution

$$\partial_u . \to \frac{1}{S_u(u)}\partial_u . \;\; ; \;\; \partial_v . \to \frac{1}{S_v(v)}\partial_v . \;\; ; \;\; \partial_w . \to \frac{1}{S_w(w)}\partial_w .$$
$$h_u(u,v,w) \to h_{tu}(u,v,w) \;\; ; \;\; h_v \to h_{tv} \;\; ; \;\; h_w \to h_{tw} \qquad \text{(II.7)}$$

Let us now introduce matrices $\boldsymbol{\Sigma}(u,v,w)$ and $\boldsymbol{\Lambda}(u,v,w)$ as

$$\Sigma(u,v,w)\equiv\begin{bmatrix} S_u h_{tu}/h_u & 0 & 0 \\ 0 & S_v h_{tv}/h_v & 0 \\ 0 & 0 & S_w h_{tw}/h_w \end{bmatrix}\begin{matrix} ¿\,u \\ ¿\,v \\ ¿\,w \end{matrix}=\begin{bmatrix} \Sigma_u & 0 & 0 \\ 0 & \Sigma_v & 0 \\ 0 & 0 & \Sigma_w \end{bmatrix}\begin{matrix} ¿\,u \\ ¿\,v \\ ¿\,w \end{matrix} \qquad \text{(II.8)}$$

$$\Lambda(u,v,w)\equiv\begin{bmatrix} \Sigma_v\Sigma_w & 0 & 0 \\ 0 & \Sigma_w\Sigma_u & 0 \\ 0 & 0 & \Sigma_u\Sigma_v \end{bmatrix}\begin{matrix} ¿\,u \\ ¿\,v \\ ¿\,w \end{matrix} \qquad \text{(II.9)}$$

Since S_u depends only on u, and similarly for S_v and S_w, the operator $\mathbf{rot}_s(.)$ (evaluated at point $(t_u(u), t_v(v), t_w(w))$) is related to operator $\mathbf{rot}(.)$ (evaluated at point (u,v,w)) by

$$\mathbf{\Lambda rot}_s.=\mathbf{rot}(\mathbf{\Sigma}.) \qquad \text{(II.10)}$$

And similarly

$$\det(\mathbf{\Sigma})\mathrm{div}_s(.)=\mathrm{div}(\mathbf{\Lambda}.) \qquad \text{(II.11)}$$

Using (II.10) and (II.11) one can reformulate the modified EM problem (II.6) as

$$\begin{cases} \mathbf{rot}\left(\mathbf{\Sigma E}_{\mathbf{PML}}\right)=-i\omega_0\left(\mathbf{\Lambda\mu\Sigma^{-1}}\right)\left(\mathbf{\Sigma H}_{\mathbf{PML}}(u,v,w)\right) \\ \mathbf{rot}\left(\mathbf{\Sigma H}_{\mathbf{PML}}\right)=+i\omega_0\left(\mathbf{\Lambda\varepsilon\Sigma^{-1}}\right)\left(\mathbf{\Sigma E}_{\mathbf{PML}}\right)+\mathbf{\Lambda j}_{\mathbf{ant}} \\ \mathrm{div}\left[\left(\mathbf{\Lambda\varepsilon\Sigma^{-1}}\right)\left(\mathbf{\Sigma E}_{\mathbf{PML}}\right)\right]=\det(\Sigma)\,\rho_{ant} \\ \mathrm{div}\left[\left(\mathbf{\Lambda\mu\Sigma^{-1}}\right)\left(\mathbf{\Sigma H}_{\mathbf{PML}}\right)\right]=0 \end{cases} \qquad \text{(II.12)}$$

Relations (II.12) can be interpreted as follows. They appear as the original electromagnetic problem (II.1), with the original differential operators $\mathbf{rot}(.)$ and $\mathrm{div}(.)$. However the original EM fields $\mathbf{E}(u,v,w)$ and $\mathbf{H}(u,v,w)$ were replaced respectively with the artificial EM fields $(\mathbf{\Sigma E}_{\mathbf{PML}})(u,v,w)$ and $(\mathbf{\Sigma H}_{\mathbf{PML}})(u,v,w)$. The original and artificial EM fields coincide inside the main simulation domain, where $\mathbf{\Sigma}=\mathbf{1}$ (the identity tensor) and $(\mathbf{E}_{\mathbf{PML}}, \mathbf{H}_{\mathbf{PML}})=(\mathbf{E}, \mathbf{H})$. Similarly the source terms ρ_{ant} and $\mathbf{j}_{\mathbf{ant}}$ were replaced respectively with $\det(\mathbf{\Sigma})\rho_{ant}$ and $\mathbf{\Lambda j}_{\mathbf{ant}}$. The original tensors $\boldsymbol{\varepsilon}$ and $\boldsymbol{\mu}$ were replaced respectively with the tensors $\boldsymbol{\varepsilon}_{\mathbf{PML}}\equiv(\mathbf{\Lambda\varepsilon\Sigma^{-1}})$ and $\boldsymbol{\mu}_{\mathbf{PML}}\equiv(\mathbf{\Lambda\mu\Sigma^{-1}})$ adapted to the stretched coordinates. Original and adapted tensors coincide in the main simulation domain, where $\mathbf{\Sigma}=\mathbf{1}$ and $\mathbf{\Lambda}=\mathbf{1}$. Also if tensor $\boldsymbol{\mu}$ is diagonal then the three matrices $\mathbf{\Lambda}$, $\boldsymbol{\mu}$ and $\mathbf{\Sigma}^{-1}$ commute. For the general dielectric tensor $\boldsymbol{\varepsilon}$ one obtains.

$$\varepsilon_{\mathbf{PML}}\equiv\mathbf{\Lambda\varepsilon\Sigma^{-1}}=\begin{bmatrix} \varepsilon_{uu}\Sigma_v\Sigma_w/\Sigma_u & \varepsilon_{uv}\Sigma_w & \varepsilon_{uw}\Sigma_v \\ \varepsilon_{vu}\Sigma_w & \varepsilon_{vv}\Sigma_w\Sigma_u/\Sigma_v & \varepsilon_{vw}\Sigma_u \\ \varepsilon_{wu}\Sigma_v & \varepsilon_{wv}\Sigma_u & \varepsilon_{ww}\Sigma_u\Sigma_v/\Sigma_w \end{bmatrix}\begin{matrix} ¿\,u \\ ¿\,v \\ ¿\,w \end{matrix} \qquad \text{(II.13)}$$

and similarly for $\boldsymbol{\mu}_{\mathbf{PML}}$. Result (II.13) is formally analogous to that in Cartesian coordinates (x, y, z) [Texeira1998], where the stretching function $S_x(x)$ was replaced with $\Sigma_u(u,v,w)$, and similarly with the other matrix components.

B. Implementation in particular geometries.

Implementation of the PML is formally similar in Cartesian and curved geometries. However the number of sub-cases is more important. For example in the case of isotropic media, one type of PML needs to be defined in Cartesian geometry, independent of the direction where waves need to be attenuated. In general 3 types of PMLs need to be defined in each direction. For anisotropic media the properties of the PML depend on both the type of

coordinates and on the orientation of the direction of anisotropy. Some of these cases are investigated below. Equation (II.13) also shows that, in curved geometry, the implementation of a PML depends on its spatial location (u,v,w) *via* the stretched coordinates $t_u(u)$, $t_v(v)$ and $t_w(w)$ appearing explicitly in $\boldsymbol{\varepsilon}_{\mathbf{PML}}$. This reflects curvature effects in the new geometry.

We now treat more explicitly four concrete examples of coordinate systems. For reference we recall the standard Cartesian set (x,y,z). One of the simplest systems exhibiting curvature is the cylindrical geometry. It is therefore useful for numerical tests, but also for simulating cylindrical plasma devices. The cylindrical coordinates (R, φ, Z) are defined as

$$\begin{cases} x = R\cos\phi \\ y = R\sin\phi \\ z = Z \end{cases} \tag{II.14}$$

For more realistic applications in tokamaks, we introduce a system of coordinates (r,φ,θ) associated to nested toric magnetic flux surfaces with concentric circular cross-sections.

$$\begin{cases} x = \left[R_0 + r\cos\theta\right]\cos\phi \\ y = \left[R_0 + r\cos\theta\right]\sin\phi \\ z = r\sin\theta \end{cases} \tag{II.15}$$

Finally we consider axisymmetric tokamak magnetic equilibria with more arbitrarily shaped nested magnetic surfaces. For simplicity, we assume that we know some conformal transformation $R+\mathrm{i}Z=F(\xi)$ in the cross-section φ=constant, such that the magnetic surfaces correspond to the images by F of circles $|\xi|=r$ in the complex plane. Properties of conformal transforms are presented *e.g.* in [Angot1972]. The existence of $F(\xi)$ is demonstrated. In magnetic fusion, conformal maps were constructed to assess numerically the magnetohydrodynamic stability of shaped toric plasmas [Goedbloed1981] [Goedbloed1982]. The coordinates (r, φ, θ) form a convenient system to locate the points in the tokamak, using

$$R+\mathrm{i}Z=F[r\exp(\mathrm{i}\theta)] \tag{II.16}$$

The conformal nature of F ensures that the original orthogonal coordinate system is transformed into another orthogonal system. The squared elementary distance reads

$$ds^2 = \left|\frac{dF\left[r\exp\left(i\theta\right)\right]}{d\xi}\right|^2\left(dr^2 + r^2 d\theta^2\right) + \mathrm{Re}\left(F\left[r\exp\left(i\theta\right)\right]\right)^2 d\phi^2 \tag{II.17}$$

The nested circular flux surfaces correspond to the translation $F(\xi)=\xi+R_0$. Table 1 summarizes the metric elements of the four coordinate systems. In the non-trivial cases, some of these elements can go to zero, leading to well-known singularities in the coordinate systems. Even when they lie outside the physical simulation domain, these singular points can be reached over the stretching process and therefore deserve special attention.

Name	u	v	w	$h_u(u,v,w)$	$h_v(u,v,w)$	$h_w(u,v,w)$
Cartesian	x	y	z	1	1	1
Cylindrical	R	φ	Z	1	R	1
Toroidal	r	φ	θ	1	$R_0+r\cos\theta$	r
Conformal	r	φ	θ	$\lvert dF/d\xi\rvert$	$\mathrm{Re}(F)$	$r\lvert dF/d\xi\rvert$

Table 1: metric elements for four coordinate systems.

III. Test problem to assess PML behaviour in cylindrical geometry.

Artificially stretching the Cartesian coordinates into the complex plane transforms propagative plane waves into evanescent ones in the PML [Sachs1995], [Gedney1996], [Texeira1998]. It therefore introduces artificial damping in this region, thus emulating radiation at infinity inside a finite simulation domain. In part II we stretched other sets of coordinates, assuming that this property might be preserved in curved geometries. However this remains to be assessed. Cylindrical geometry is a well suited test case.

A standard assessment of the PML formulation in Cartesian geometry is to quantify the reflection of propagative or evanescent plane waves in homogeneous media (see *e.g.* [Jacquot2013]). In cylindrical coordinates some equivalents of propagating or evanescent plane waves exist in terms of Bessel functions. In the context of plasma-filled waveguides, these cylindrical waves were derived in details for gyrotropic media in [Bers1963]. These results are briefly summarized in section III.A in the case of longitudinal anisotropy. Using these tools we then propose a test problem to analytically quantify the reflection of cylindrical waves by radial PMLs in cylindrical geometry, in presence of a homogeneous gyrotropic medium. We investigate in particular how the radial curvature of the cylinder affects the PML properties compared to the Cartesian case.

A. Cylindrical waves in gyrotropic medium with longitudinal anisotropy.

From now on we seek particular solutions of the wave equations (II.1), without source term in volume, featuring a separable form in the cylindrical coordinates (R, φ, Z). The EM quantities are requested to oscillate as $F(R)\exp(+i\omega_0 t - ik_z Z - im\varphi)$, with k_z a longitudinal wavevector, m (integer) an azimuthal mode number, and $F(R)$ a radial structure function to be determined. For gyrotropic media these cylindrical waves can only be well defined when the direction of anisotropy is along Z or φ [Bers1963]. For convenience we summarize here Bers' treatment in the homogeneous medium with longitudinal anisotropy (see also [Swanson2003]). This geometry is well suited for magnetized cylindrical plasma devices, in conditions when longitudinal invariance can be assumed. In this configuration $\boldsymbol{\mu}(\omega_0)=\mu_0\mathbf{1}$ in formula (II.2) while the dielectric tensor $\boldsymbol{\varepsilon}(\omega_0)$ takes the form [Swanson2003]

$$\frac{\varepsilon(\omega_0)}{\varepsilon_0}=\begin{bmatrix} \varepsilon_{\perp}(\omega_0) & +i\varepsilon_{\perp}(\omega_0) & 0 \\ -i\varepsilon_{\perp}(\omega_0) & \varepsilon_{\perp}(\omega_0) & 0 \\ 0 & 0 & \varepsilon_{//}(\omega_0) \end{bmatrix} \begin{matrix} \leftarrow R \\ \leftarrow \phi \\ \leftarrow Z \end{matrix} \qquad \text{(III.1)}$$

In this configuration all the EM field components $\mathbf{E}_T(R)$ and $\mathbf{H}_T(R)$ transverse to Z can be expressed as a function of the longitudinal EM field components $E_Z(R)$ and $H_Z(R)$ using Maxwell-Ampère and Maxwell-Faraday equations ([Bers1963], eq. 9.21)

$$\begin{bmatrix} E_T(R) \\ H_T(R) \end{bmatrix} = \frac{k_0^{-1}}{\left(\varepsilon_{\square}-n_Z^2\right)^2-\varepsilon_{\times}^2} \times \dots$$

$$\begin{bmatrix} -in_Z\left(\varepsilon_{\square}-n_z^2\right) & Z_0\varepsilon_{\times} & n_Z\varepsilon_{\times} & +iZ_0\left(\varepsilon_{\square}-n_z^2\right) \\ -Z_0^{-1}n_Z^2\varepsilon_{\times} & -in_Z\left(\varepsilon_{\square}-n_z^2\right) & -iZ_0^{-1}\left(\varepsilon_{\square}^2-\varepsilon_{\times}^2-n_z^2\varepsilon_{\times}\right) & n_Z\varepsilon_{\times} \end{bmatrix} \begin{bmatrix} \square_T E_Z \\ \square_T H_Z \\ e_Z \times_T E_Z \\ e_Z \times_T H_Z \end{bmatrix} \qquad \text{(III.2)}$$

In the above expression we have introduced $c=[\mu_0\varepsilon_0]^{-1/2}$ the speed of light in vacuum, $k_0\equiv\omega_0/c$ the wave-vector in vacuum, $n_Z\equiv k_Z/k_0$ the longitudinal refractive index and $Z_0=(\mu_0/\varepsilon_0)^{1/2}$

the impedance of vacuum. In our cylindrical geometry the relevant 2D transverse operator is $\nabla_T \cdot = \begin{bmatrix} \partial_R \cdot \\ -\Im/R \end{bmatrix} \begin{matrix} ¿R \\ ¿\phi \end{matrix}$ so that $e_z \times \nabla_T \cdot = \begin{bmatrix} \Im/R \\ \partial_R \cdot \end{bmatrix} \begin{matrix} ¿R \\ ¿\phi \end{matrix}$. Substituting (III.2) into Maxwell's equations, the two scalar fields $E_Z(R)$ and $H_Z(R)$ are then related to each other by two coupled second-order partial differential equations ([Bers1963], eq. 9.157 and 9.158)

$$\Delta_T \begin{bmatrix} E_Z \\ H_Z \end{bmatrix} + k_0^2 K \begin{bmatrix} E_Z \\ H_Z \end{bmatrix} = 0 \qquad \text{(III.3)}$$

In this expression Δ_T. is the Laplace operator transverse to anisotropy while matrix **K** takes the form

$$K \equiv \begin{bmatrix} \varepsilon_{¿}/¿\left(1-n_Z^2/\varepsilon_{❑}\right)¿ & -i Z_0 n_Z \varepsilon_\times ¿ \varepsilon_{❑} \\ i n_Z \varepsilon_\times \varepsilon_{¿}/¿¿ Z_0 \varepsilon_{❑} ¿ \varepsilon_{❑} & -\varepsilon_\times^2/\varepsilon_{❑} - n_Z^2 \end{bmatrix} \qquad \text{(III.4)}$$

Eigenmodes of the gyrotropic medium are the eigenvectors of matrix **K,** associated with eigenvalues $n_\perp^2$, a squared refractive index transverse to Z. The dispersion relation for cylindrical waves writes

$$\det\left(K - n_¿^2 1\right) = n_¿^4 - \mathrm{tr}\left(K\right) n_¿^2 + \det K = 0 \qquad \text{(III.5)}$$

Two separate roots $n_\perp^2$ generally fulfil equation (III.5). Below we will investigate only media without losses in volume, for which the three dielectric constants in (III.1) are real, but without restriction of sign. In these conditions the eigenvalues $n_\perp^2$ are also real. When $n_z\varepsilon_\times/\varepsilon_\perp=0$ matrix **K** is diagonal and the EM fields can be explicitly split into transverse-electric (TE) and transverse-magnetic (TM) eigenmodes with respect to direction Z

$$\begin{cases} n_{¿TM}^2 = K_{11} = \varepsilon_{//}\left(1 - n_Z^2 ¿ \varepsilon_{¿}\right) \\ n_{¿TE}^2 = K_{22} = \varepsilon_{¿} - \varepsilon_{¿}^2 ¿ \varepsilon_{¿} - n_Z^2 \end{cases} \qquad \text{(III.6)}$$

In our numerical tests we will also investigate EM waves for magneto-plasmas in the Ion Cyclotron Range of Frequencies (ICRF) [Swanson2003]. Such waves satisfy the ordering $|\varepsilon_{//}| >> |\varepsilon_\perp|, |\varepsilon_\times|, n_Z^2$. A scale separation generally applies, allowing a perturbative resolution of (III.5). To leading order in the ordering the refractive indices are

$$\begin{cases} n_{¿FW}^2 \approx \det(K)/\mathrm{tr}(K) = \left[\left(\varepsilon_{¿} - n_Z^2\right)^2 - \varepsilon_{¿}^2\right] / \left(\varepsilon_{¿} - n_Z^2\right) \\ n_{¿SW}^2 \approx \mathrm{tr}(K) = \varepsilon_{//}\left(1 - n_Z^2/\varepsilon_{¿}\right) \end{cases} \qquad \text{(III.7)}$$

Scale separation fails close to $n_z^2=\varepsilon_\perp$. Within the above ordering, the polarization of the first mode (Fast Wave or FW in ICRF) is quasi-TE.

$$\frac{E_{Z,FW}}{H_{Z,FW}} = \frac{-K_{12}}{K_{11} - n_F^2} \approx i Z_0 \frac{n_Z \varepsilon_\times}{\varepsilon_{¿}/¿\left(\varepsilon_{❑} - n_Z^2\right)¿} \qquad \text{(III.8)}$$

The polarization of the alternative eigenmode (Slow Wave or SW) is to leading order

$$\frac{H_{Z,FW}}{E_{Z,FW}} = \frac{-K_{21}}{K_{22} - n_S^2} \approx i \frac{n_Z \varepsilon_\times}{Z_0\left(\varepsilon_{❑} - n_Z^2\right)} \qquad \text{(III.9)}$$

For eigenmodes the two equations (III.3) simplify into two scalar Helmholtz equations

$$\Delta_T H_Z(R)+k_\zeta^2 H_Z(R)=0 \quad ; \quad k_\zeta^2=k_0^2 n_\zeta^2 \qquad \text{(III.10)}$$

and similarly for $E_Z(R)$. In our cylindrical coordinates, $\Delta_T=R^{-1}\partial_R R\partial_R-m^2/R^2$ and (III.10) is a Bessel equation. When $n_\perp^2$ is real positive, solutions of (III.10) with radiation conditions at infinity are found as Hankel functions $H_m^{(1)}(k_\perp R)$ and $H_m^{(2)}(k_\perp R)$ [Abramowitz]. For $|k_\perp R|>>1$, $H_m^{(1)}(k_\perp R)\sim[2/(\pi k_\perp R)]^{1/2}\exp(+ik_\perp R-i\pi/4-im\pi/2)$, *i.e.* taking $k_\perp$ real positive this wave behaves asymptotically as a plane wave propagating radially inwards. Similarly $H_m^{(2)}(k_\perp R)\sim[2/(\pi k_\perp R)]^{1/2}\exp(-ik_\perp R-i\pi/4-im\pi/2)$ propagates in the outward direction. Evanescent waves with real negative $n_\perp^2$ can be treated similarly by replacing $H_m^{(1)}$ and $H_m^{(2)}$ with respectively the modified Bessel functions I_m and K_m of argument $|k_\perp|R$ [Abramowitz].

Once $E_Z(R)$ and $H_Z(R)$ are determined for each eigenmode, the transverse parts of their EM field polarizations are deduced from (III.2). Finally, the full solution of the initial EM problem (II.1) is a linear combination of the two eigenmodes determined by the source terms and boundary conditions. If a cylindrical Perfect Electric Conductor (PEC) is present at $R=R_1$, the two EM field components $E_Z(R_1)$ and $E_\varphi(R_1)$ tangent to this boundary should vanish simultaneously. In the general case treated in [Bers1963], a mix of the two eigenmodes is needed to fulfil the PEC boundary conditions, leading to mode conversion upon wave reflection. However in the case of pure TE or TM modes, solutions exist involving only one of the two eigenmodes. This is also approximately the case for the FW at leading order in the above ordering. For our test problem we will stick to these simple cases.

B. Reflection of propagative cylindrical TE Waves in a Radial PML.

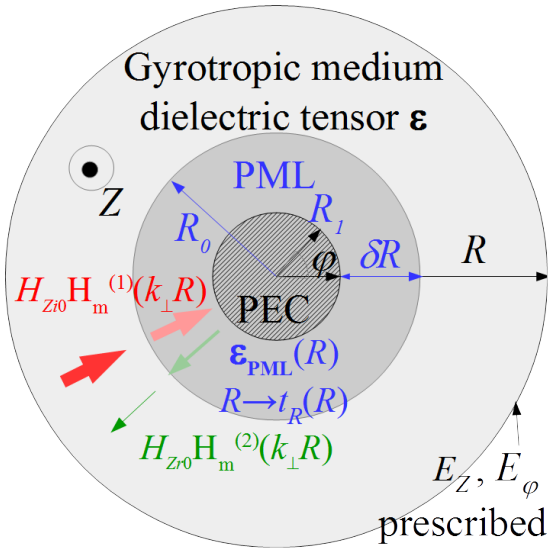

Figure 1: sketch of TE wave reflection problem to assess the radial PML.

To assess the behaviour of radial PMLs in cylindrical geometry, we study the artificial damping of an incoming propagative cylindrical TE wave in the central part of a homogeneous gyrotropic medium with longitudinal aniosotropy. This situation mimics the complete absorption of a TE wave launched from the periphery of a cylindrical magnetized plasma device. The geometry of our test problem is summarized on figure 1. An incident cylindrical TE wave is launched from $R\to+\infty$ towards $R=0$. To attenuate artificially this incoming wave near the centre of the cylinder, a radial PML is placed in a cylindrical shell between $R=R_1$ and $R=R_0=R_1+\delta R$. Inside the PML the radial coordinate R is stretched into $t_R(R)$. Although this choice is non-restrictive, we will discuss below the particular case of polynomial stretching functions, for easier comparison with earlier work in Cartesian coordinates [Jacquot2013]. Specifically

$$S_R(R)=1-(S'+iS'')[|R-R_0|/\delta R]^p,\ R<R_0 \qquad \text{(III.11)}$$

From this one can define $t_R(R)$ explicitly as

$$R\to t_R(R)=R+\frac{S'+iS''}{p+1}\left(\frac{R_0-R}{\delta R}\right)^{p+1}\delta R \qquad \text{(III.12)}$$

The other two cylindrical coordinates (φ, Z) are not stretched. From the above calculations, and assuming here $k_{\perp TE}^2>0$, the radial structure of the incoming longitudinal EM magnetic field in the PML takes the form

$$H_{ZiPML}(R)=H_{Zi0}H_m^{(1)}[k_{\perp TE}t_R(R)] \qquad \text{(III.13)}$$

where the (complex) stretched radial coordinate $t_R(R)$ was substituted to the (real) radius R. The coordinate stretch preserves the TE polarization for the artificial EM electric field $\mathbf{E}_{\mathbf{PML}}$. A PEC is placed in $R=R_1<R_0$. Other boundary conditions are possible there (*e.g.* Perfect Magnetic Conductor would be convenient for TM modes). At this radius the total tangential EM electric field should vanish. In the case of the TE modes $E_{ZPML}=0$ and one should cancel only the azimuthal component $E_{\varphi PML}(R_1)$. This can be fulfilled with only incident and reflected TE waves sharing the same (k_z, m), so that the alternative eigenmode is absent from the problem. The reflected TE wave adopts a radial structure function of the form

$$H_{ZrPML}(R)=H_{Zr0}H_m^{(2)}[k_{\perp TE}t_R(R)] \qquad \text{(III.14)}$$

From equation (III.2), $E_{\varphi PML}(R_1)=0$ means

$$\frac{H_{Zr0}}{H_{Zi0}}=\eta_{theo}=-\frac{-m\varepsilon_{\times}H_m^{(1)}\left[k_{\times}t_R(R_1)\right]+\left(\varepsilon_{\times}-n_Z^2\right)k_{\times}t_R(R_1)H_m^{'}\left[k_{\times}t_R(R_1)\right]}{-m\varepsilon_{\times}H_m^{(2)}\left[k_{\times}t_R(R_1)\right]+\left(\varepsilon_{\times}-n_Z^2\right)k_{\times}t_R(R_1)H_m^{'}\left[k_{\times}t_R(R_1)\right]} \qquad \text{(III.15)}$$

In this expression the primes denote the derivative of the Hankel functions with respect to their arguments, and subscript TE was dropped. Equation (III.15) defines an amplitude reflection coefficient η_{theo} for the TE modes, whose magnitude can be used as a figure of merit for assessing the PML. In the absence of coordinate stretching ($t_R(R)=R$) the PML is replaced with an equivalent layer of gyrotropic material and $|\eta_{theo}|=1$. The coordinate stretching in the PML aims at reducing $|\eta_{theo}|$ as much as possible.

η_{theo} depends on the wave characteristics (k_0, n_z, m), the dielectric tensor elements, the PML characteristics (S', S'', δR, p) as well as the PEC radial location R_1. The situation is therefore more complex than in Cartesian geometry. However only three independent non-dimensional parameters appear in formula (III.15): the complex argument $k_{\perp}t_R(R_1)$ in the Hankel functions, the ratio $m\varepsilon_{\times}/(\varepsilon_{\perp}-n_Z^2)$ and the azimuthal mode number m. Coordinate stretching only influences the first parameter. To shed light into the PML properties, we therefore investigate below the quantities $|\eta_1|=|H_m^{(1)}[k_{\perp}t_R(R_1)]/H_m^{(2)}[k_{\perp}t_R(R_1)]|$ and $|\eta_2|=|H_m^{'(1)}[k_{\perp}t_R(R_1)]/H_m^{'(2)}[k_{\perp}t_R(R_1)]|$. They correspond to $|\eta_{theo}|$ for respectively very large or very small values of $m\varepsilon_{\times}/(\varepsilon_{\perp}-n_Z^2)$. For increasing m, figures 2 plot $|\eta_1|$ and $|\eta_2|$ versus the two non-dimensional real parameters (X_{PML}, Y_{PML}) appearing in the Hankel functions:

$$\begin{cases} X_{PML}\equiv \mathrm{Re}\left[k_{\times}t_R(R_1)\right]=k_{\times}\left[R_1+\delta R\,S'/(p+1)\right] \\ Y_{PML}\equiv \mathrm{Im}\left[k_{\times}t_R(R_1)\right]=k_{\times}\delta R\,S''/(p+1) \end{cases} \qquad \text{(III.16)}$$

Parameter Y_{PML} is similar to the one characterizing the efficiency of the Cartesian PML for propagating plane waves [Jacquot2013], where in this context subscript $\perp$ means normal to the plasma/PML interface.

$|\eta_{theo}|=1$ for $Y_{PML}=0$ and $X_{PML}>0$. Since $H_m^{(1)}[X_{PML}-iY_{PML}]=H_m^{(2)}[X_{PML}+iY_{PML}]^*$ (where * denotes complex conjugate), η_{theo} is transformed into $1/\eta_{theo}^*$ when $Y_{PML}\rightarrow -Y_{PML}$. Concretely this means that the PML cannot be tuned to attenuate simultaneously EM waves with real positive and real negative $k_{\perp}$. As discussed in [Jacquot2013] [Bécache2017] this might be problematic in some anisotropic media where propagative forward and backward waves can coexist. Figures 2 plot only the half-plane $Y_{PML}>0$.

Taking $Y_{PML}>0$ generally reduces $|\eta_{theo}|$, but not always: contrary to the equivalent Cartesian PML $|\eta_{theo}|$ can exceed 1 and reach very high values for positive Y_{PML}. This arises when $E_{\varphi PML}(R_1)=0$ for the reflected wave. $|\eta_1|$ reaches very high values near the complex zeros of $H_m^{(2)}$, and similarly for $|\eta_2|$ near the complex zeros of $H'_m{}^{(2)}$. For $m=0$ these zeros all lie in the half-plane $X_{PML}<0$. As m increases some zeros are progressively displaced towards $X_{PML}>0$. It is therefore important to tune S' so that this zone of the complex space is avoided.

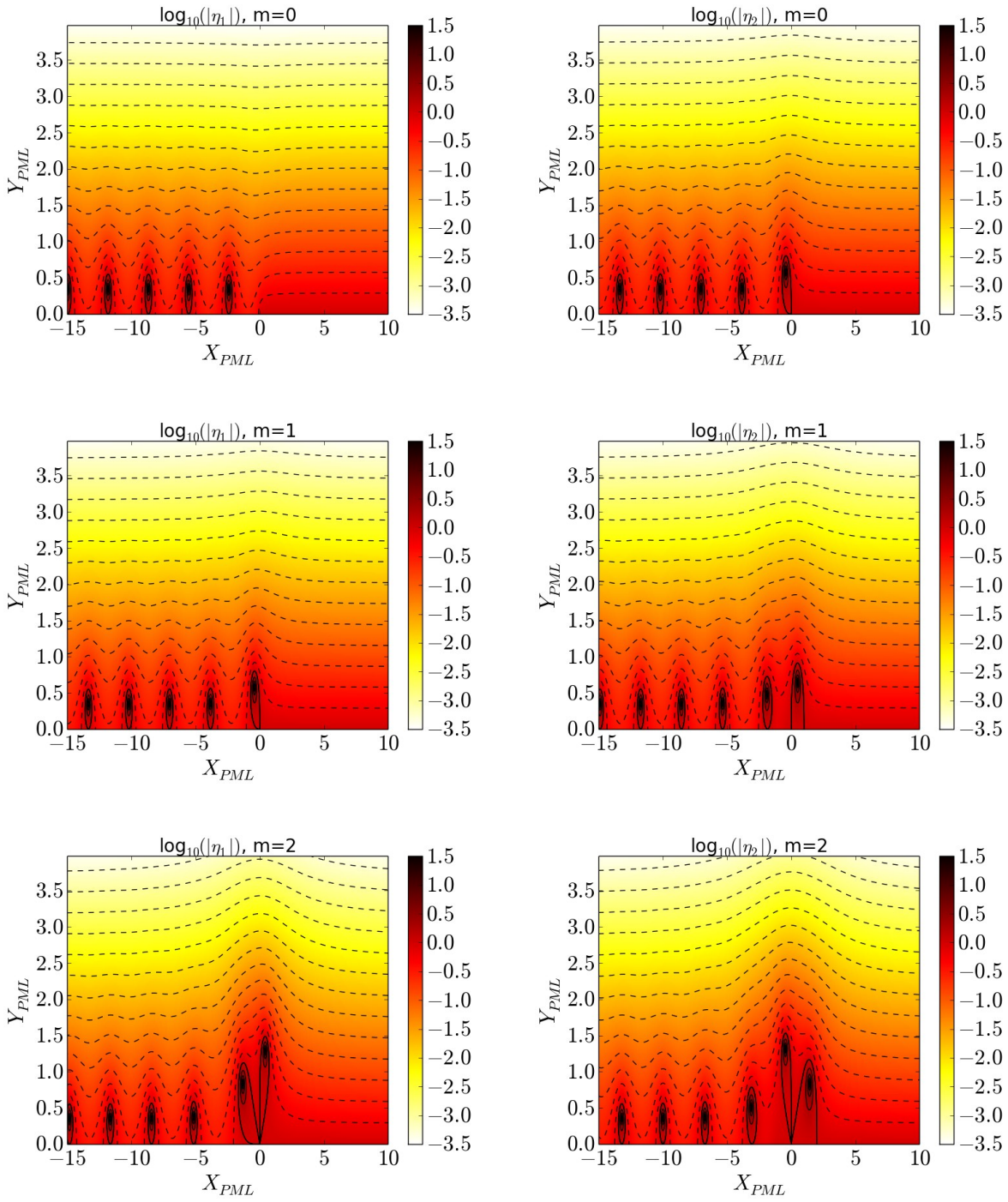
log10(|η1|), m=0
log10(|η2|), m=0
log10(|η1|), m=1
log10(|η2|), m=1
log10(|η1|), m=2
log10(|η2|), m=2
YPML
XPML

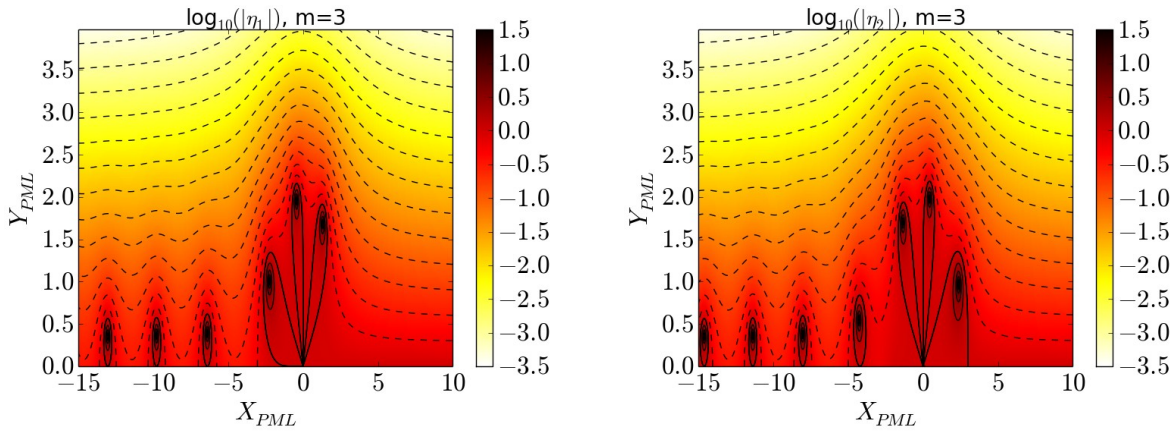

Figure 2: 2D Contour plots of $|\eta_1|$ (left panels) and $|\eta_2|$ (right panels) in logarithmic scale versus X_{PML} and Y_{PML}, from formula (III.16), for increasing azimuthal mode number m. One contour line every 2.5dB. First solid contour line corresponds to $|\eta|=1$.

Unlike the Cartesian case, the PML properties for propagative cylindrical waves depend on X_{PML}. This parameter can be seen as a normalized radial position of the PEC boundary in the stretched coordinates. X_{PML} can change either by moving physically the PEC radius R_1 or by acting on the stretching parameters $\delta RS'/(p+1)$. The second method amounts to artificially displacing the PEC radial position towards a region of different radius (even possibly negative!). The dependence of η_{theo} on X_{PML} can be interpreted in terms of local curvature effects at the stretched PML location.

In the limit of large $|X_{PML}+iY_{PML}|$ with positive X_{PML} one finds [Abramowitz]

$$|H_m^{(1)}[X_{PML}+iY_{PML}]/H_m^{(2)}[X_{PML}+iY_{PML}]|\sim$$
$$|H_m'^{(1)}[X_{PML}+iY_{PML}]/H_m'^{(2)}[X_{PML}+iY_{PML}]|\sim\exp(-2Y_{PML})\equiv|\eta_{Cart}| \qquad \text{(III.17)}$$

i.e. $|\eta_1|$, and $|\eta_2|$, and therefore $|\eta_{theo}|$ as well, converge to the same value $|\eta_{Cart}|$, independent of (X_{PML}, m) and characteristic of Cartesian PMLs [Jacquot2013]. However the minimal Y_{PML} to reach this asymptotic regime depends on (X_{PML}, m): the higher m and the lower X_{PML}, the higher Y_{PML} should be.

The parametric region around $X_{PML}+iY_{PML}=0$ appears unfavourable for low wave reflection by the PML. Low values of X_{PML} and Y_{PML} are reached for low ($k_\perp\delta R$), *i.e.* for waves propagating nearly parallel to the plasma/PML interface, similar to the Cartesian case [Jacquot2013]. The size of the unfavourable region gets larger as m increases: for given (X_{PML},Y_{PML}), a critical value of m always exists above which the PML loses efficiency. Figures 3 map as a function of (X_{PML},Y_{PML}) the lowest value of m for which the amplitude ratio exceeds 0.1. In figures 3 this value is $m=0$ for $Y_{PML}<1.2$. The critical m value increases with both X_{PML} and Y_{PML}. It can therefore be made arbitrarily high by proper PML tuning. In practical applications, only a finite number of azimuthal harmonics need to be resolved. The PML can always be tuned so that it remains efficient up to this maximum m. In particular stretching the real part of R can be beneficial if it moves artificially the PEC location towards regions of lower curvature. Larger coordinate stretching however produces larger radial variations of $\boldsymbol{\varepsilon}_{\mathbf{PML}}(R)$ and therefore imposes a finer discretization of the PML region.

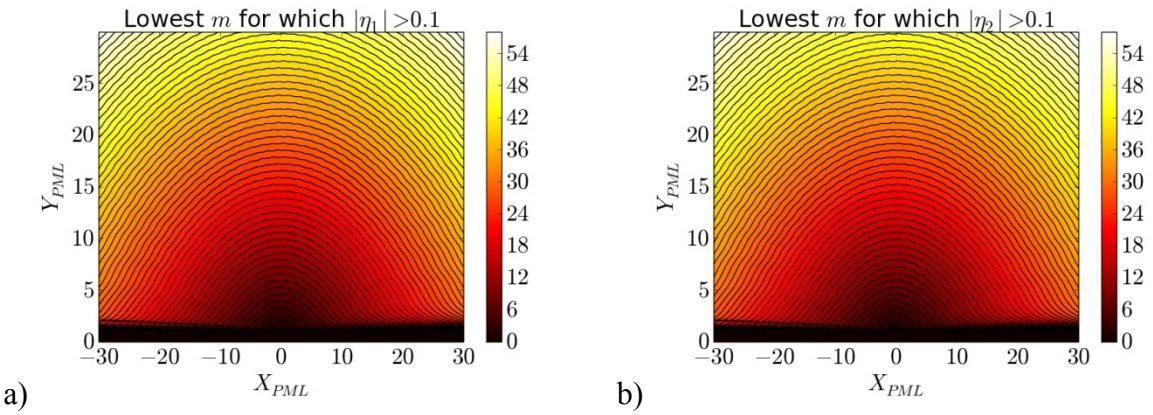

Figure 3: lowest value of azimuthal mode number m for which the amplitude ratios exceeds 0.1, versus (X_{PML},Y_{PML})*. a)* $|\eta_1|>0.1$*, b)* $|\eta_2|>0.1$*.*

C. Reflection of evanescent cylindrical waves in a radial PML.

When $k_\perp^2$ is real negative for the TE mode, a similar analysis as before can be made for waves that are evanescent inwards, *i.e.* waves growing radially as $\exp(+|k_\perp|R)$ for large R. In formula (III.15) functions $H_m^{(1)}$ and $H_m^{(2)}$ should be respectively replaced with I_m and K_m [Abramowitz]. In the absence of coordinate stretching, the equivalent of η_1 writes $K_m(X_1)/I_m(X_1)$, where $X_1=|k_\perp|R_1$ is a real normalized radius at PEC location. After the stretching, argument X_1 should be transformed into $X_1+\delta X_{PML}+i\delta Y_{PML}$ where

$$\begin{cases} \delta X_{PML} \equiv |k_\iota| \delta R\, S'/(p+1) \\ \delta Y_{PML} \equiv |k_\iota| \delta R\, S''/(p+1) \end{cases} \qquad \text{(III.18)}$$

Figures 4 therefore plot the ratio $|\eta_3|=|K_m(X_1+\delta X_{PML}+i\delta Y_{PML})/I_m(X_1+\delta X_{PML}+i\delta Y_{PML})|*I_m(X_1)/K_m(X_1)$ *versus* $(\delta X_{PML},\delta Y_{PML})$. Only positive δY_{PML} are shown since negative δY_{PML} produce a similar result. $|\eta_3|$ is 1 for $(\delta X_{PML},\delta Y_{PML})=(0,0)$ and should be ideally as low as possible. For given δY_{PML}, $\delta X_{PML}>0$ is always beneficial for attenuating the reflected wave compared to $\delta X_{PML}=0$, while $\delta X_{PML}<0$ might be very detrimental, especially close to $\delta X_{PML}=-X_1$. For positive δX_{PML}, adding δY_{PML} is generally beneficial but not always. For large positive X, $|K_m(X+iY)/I_m(X+iY)|\sim\exp(-2X)/2|X+iY|$ and one recovers a result similar to the Cartesian case.

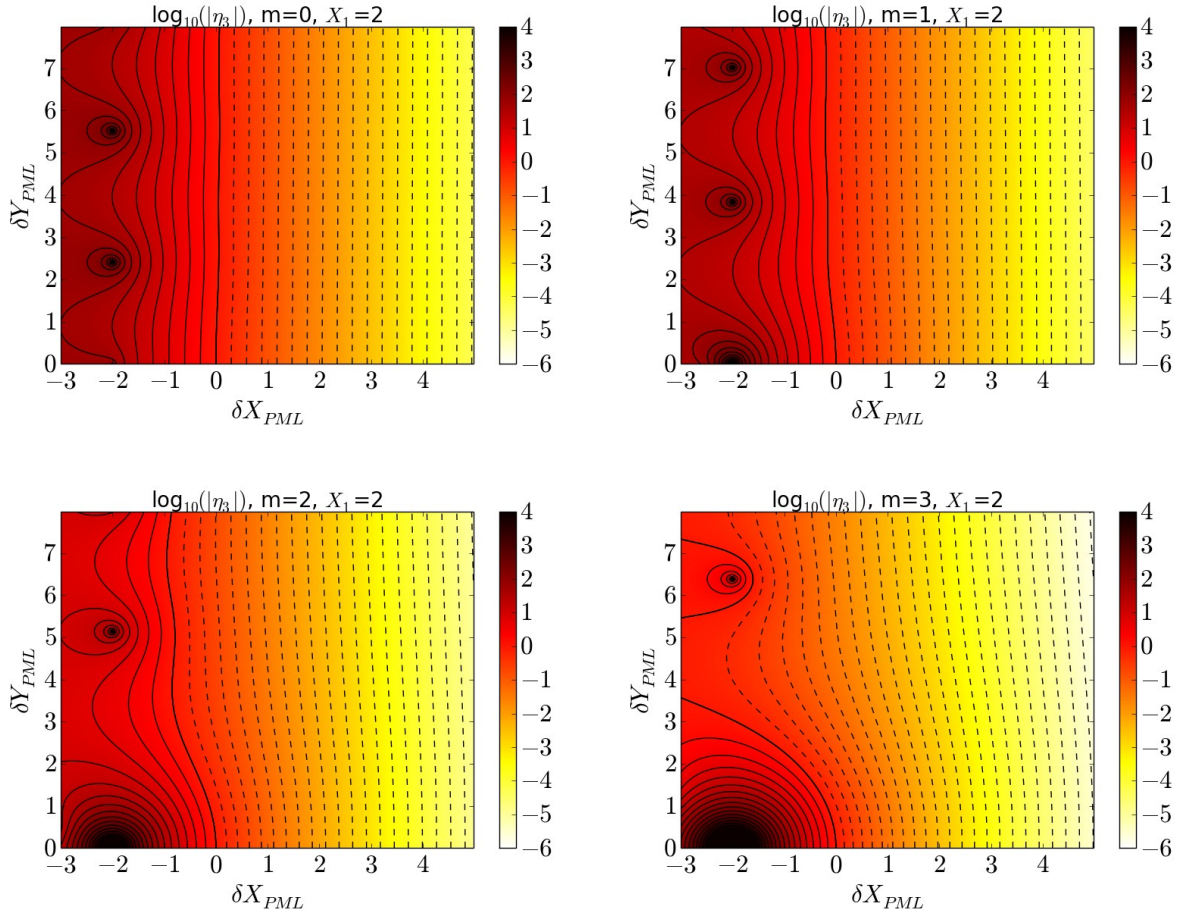

Figure 4: 2D contour plots of amplitude ratio $|\eta_3|$ (in logarithmic scale) versus (δX_{PML},δY_{PML}) from (III.18) for X_1=2.0 and for the first four values of azimuthal mode number m. One contour line every 2.5dB. First solid contour line corresponds to $|\eta_3|$=1.

IV. Numerical tests of radial PML with gyrotropic media using 2D finite elements.

The test problem for propagative cylindrical TE waves proposed in part III was implemented with finite elements in two dimensions (2D), and the wave reflection was quantified from the simulation output. This allows assessing numerically the analytical figure of merit η_{theo} from (III-15). Simulations also illustrate specific features and limitations of the PML in cylindrical geometry and outline practical tips for PML tuning.

A. Simulation and post-processing protocols

Using the COMSOL finite element solver [COMSOL], the test problem was simulated numerically in the 2D (radial, azimuthal) geometry (R,φ) sketched on figure 1, with EM fields assumed to vary as $\exp(-ik_zZ)$ in the out-of-plane longitudinal direction Z. COMSOL includes a built-in module to simulate the standard EM problem (II.1) with standard boundary conditions and any user-defined material of type (II.2), possibly inhomogeneous in space. All over the main simulation domain, the homogeneous gyrotropic dielectric tensor (III.1) was applied. A PML was implemented in the inner part of the simulation domain. When not precised, the artificial inhomogeneous tensors $\boldsymbol{\varepsilon}_{\mathbf{PML}}(R)$ and $\boldsymbol{\mu}_{\mathbf{PML}}(R)$ from (II.13) were applied there, where $\boldsymbol{\varepsilon}$ is still from (III.1) and the radial coordinate R was stretched according to formula (III.12). From table 1, matrix $\boldsymbol{\Sigma}(R)$ in formula (II.8) takes the form

$$\boldsymbol{\Sigma}(R)=\begin{bmatrix} S_R(R) & 0 & 0 \\ 0 & t_R(R)/R & 0 \\ 0 & 0 & 1 \end{bmatrix}_{R,\varphi,Z} \qquad \text{(IV.1)}$$

It differs from a Cartesian-like PML formulation by a non-trivial term $\Sigma_\varphi(R)=t_R(R)/R$ in the azimuthal direction. The PML medium features complex dielectric tensor elements, introducing artificial losses in PML volume. Besides, the three diagonal elements of $\boldsymbol{\varepsilon}_{\mathbf{PML}}(R)$ are different from each other and $\boldsymbol{\mu}_{\mathbf{PML}}(R)$ becomes non-trivial. A PEC was implemented at the inner radial boundary of the simulation domain. From equation (II.12) this boundary condition applies to the EM field $\boldsymbol{\Sigma}\mathbf{E}_{\mathbf{PML}}$ computed in the PML. Since matrix $\boldsymbol{\Sigma}(R)$ is diagonal in (IV.1), this amounts to cancelling both $E_{\varphi PML}$ and E_{ZPML} all over the inner radial boundary.

Several simulation series, summarized in table 2, scanned the plasma and PML parameters identified as important in section III.

#	f_0 [MHz]	k_z [m^{-1}]	m	$\varepsilon_\perp$	$\varepsilon_\times$	S'	S"	p	R_1 [m]	δR [m]
1	50	0	0	40.0	0.0	-2.0	-1.0 +7.0	2	0.5	0.5
2	50	0	0	40.0	0.0	+2.0	3.0	2	0.5	0.05 1.2
3	50	0	0	10.0 810	0.0	+2.0	1.5	2	0.5	0.5
4	25.0 225.0	0	0	40.0	0.0	-4.0	1.5	2	0.5	0.5
5	50	0	0 19	40.0	0.0	+2.0	1.0	2	0.5	0.5
6	50	0	6	40.0	0.0	-4.0 +2.0	1.12	2	0.5	0.5
7	100	0.0 12.0	7	40.0	0.0	3.0	2.0	2	0.5	0.5
8	100	0.0	4	40.0	0.0	0.0	0.55	2	0.05 1.5	0.5
9	100	0.0	4	40.0	0.0	-6.39 +6.1 2	0.55	2	0.23	0.5
10	50	0.0	0	40.0	0.0	2.0	2.0	0 5	0.5	0.5
11	50	0.0	0	750. 0	-735 0	2.0	1.5	2	0.5	0.5
12	50	30.0	0	1500	-672 0	2.0	1.5	2	0.5	0.5
13	50	0.0	3	750. 0	-740 +740	2.0	1.5	2	0.5	0.5
14	50	30.0	4	1500	-680 +680	2.0	1.5	2	0.5	0.5

Table 2: overview of parametric space explored over the simulations. Scanned parameters are highlighted in green. In series 1-11, $\varepsilon_{//}$=-10^5 was used but should not play any role. In simulation series #12 and #14 highlighted in grey the TE polarization is only approximate. Series 12 was performed using $\varepsilon_{//}$=-10^6 and $\varepsilon_{//}$=-10^7. Series 13 and 14 were performed with $\varepsilon_{//}$=-10^6 and $\varepsilon_{//}$=-10^8.

Only cases with propagative cylindrical waves were envisaged. The cases considered also feature $\varepsilon_\times=0$ or highly negative $\varepsilon_{//}$, so that the EM problem (II.12) involves only (or mainly) the TE mode. TE wave polarization is exact for all series except #12 and #14 highlighted in grey, where it is approximate since $k_z\varepsilon_\times\neq 0$. Consistent with this assumption the longitudinal EM electric field E_Z was imposed null at the outer boundary of the simulation domain, except on series #12 and #14, where the approximate formula (III.8) was used for the FW polarization. The prescribed azimuthal EM electric field at this location was $E_\varphi(R,\varphi)=E_0\exp(-im\varphi)$ to select the proper azimuthal mode number. The outer boundary of the simulation domain was always located 1 m outside the PML outer radius. For the sake of comparison, series #1 of table 2 was also repeated using a Cartesian-like PML formulation, where $\Sigma_\varphi(R)=1$ was imposed in (IV.1), *i.e.* the effect of the cylindrical curvature was artificially suppressed. Both the main simulation domain and the PML were discretized using an unstructured mesh of quadratic triangular finite elements, with typical size 1cm. Up to 843474 elements were necessary to mesh the largest simulation domains, corresponding to 5908342 degrees of freedom. Calculations relied on the direct solver MUMPS.

In order to numerically assess the reflection of propagating cylindrical waves by the PML, the azimuthal average of $H_Z(R,\varphi)\exp(im\varphi)$ was extracted from the 2D simulation output in the main simulation domain. Using a least-square procedure, the radial variation of this quantity was fitted with a linear combination of $H_m^{(1)}(k_\perp R)$ and $H_m^{(2)}(k_\perp R)$, with respective complex weights H_{Zi0_sim} and H_{Zr0_sim}. In the argument of the Hankel functions, dispersion relations (III.6) or (III.7) were used to determine $k_\perp$ from the input parameters. Finally the magnitude of the simulated amplitude ratio $\eta_{sim}=H_{Zr0\_sim}/H_{Zi0\_sim}$ served as a figure of merit to quantify the PML reflection in the numerical tests. The fitting procedure implicitly assumes that only the TE mode with correct m is present in the simulation. In practice numerical noise is always superimposed to the ideal results, as well as the other eigenmode of the gyrotropic medium, especially in the cases where the TE polarization is only an approached input. Besides, dispersion relation (III.7) is only approximate. All this introduces uncertainties in the numerical determination of η_{sim}.

B. Comparison with analytical figure of merit.

Over the simulation database, Figures 5 compare the numerical reflection coefficient η_{sim} with theoretical expectation η_{theo} from formula (III.15). An important restriction to the allowed parametric space will be discussed on Figure 6 and is excluded here. $|\eta_{sim}|$ values well above 1 could be reached, indicating that the reflected wave can be amplified by the PML instead of being attenuated. This situation is met when the imaginary part S'' of the stretching is negative, like in the Cartesian case. For positive S'', this might also be the case for some values of X_{PML} in formula (III.16), a specificity of the cylindrical geometry producing the peaks on figures 2. η_{sim} agrees well with η_{theo} over eight orders of magnitude down to reflection levels of 10^{-5}, when the precision of the simulation gets limited by either the mesh size or the fitting procedure. The relative difference between η_{sim} and η_{theo} roughly scales as $1/\min(|\eta_{theo}|, |\eta_{theo}|^{-1})$. This relative difference is significantly enhanced in simulation series #12 and #14 with $k_z\varepsilon_\times\neq 0$. We speculate this is not due to the PML but because we used approximated boundary conditions for the quasi-TE polarization: while the simulation points with $\varepsilon_{//}=-10^7$ or $\varepsilon_{//}=-10^8$ appear in the ballpark of the other series on figure 5.b, the runs with $\varepsilon_{//}=-10^6$ are well above.

Figures 5 also show a repeat of series #1 in table 2, using a Cartesian-like formulation of the PML. In this series $|\eta_{sim}|=1$ for $S''=0$, as it should for energetic reasons. For some values of S'', the Cartesian-like PML behaves better than the cylindrical one. This is however observed over a limited window in parametric space, and it is hardly predictable in advance.

For large S'', the simulated amplitude reflection coefficient reaches an asymptotic value above 10^{-2}, while the cylindrical PML achieves $|\eta_{sim}|<10^{-5}$. This illustrates the merits of the new PML formulation in curved coordinates.

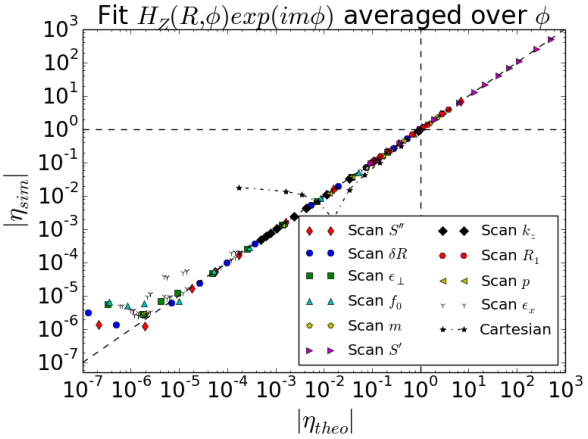

Figure 5.a): numerical amplitude reflection coefficient $|\eta_{sim}|$ versus theoretical value $|\eta_{theo}|$ expected from formula (III.15), over simulation series #1-#14 from table 2. Last series: same as series #1, using a Cartesian PML-like PML formulation, with $\Sigma_\varphi(R)=1$ artificially imposed in formula (IV.1)

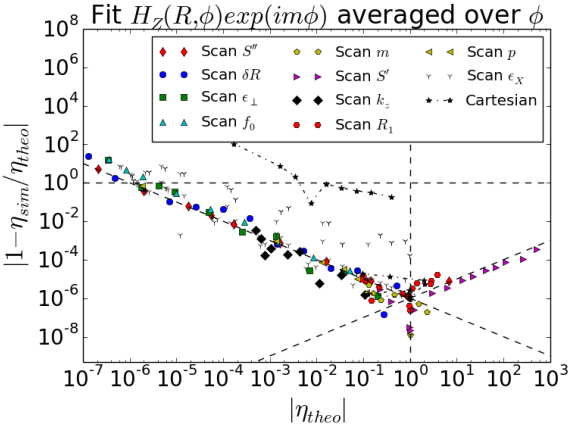

Figure 5.b): Same database as figure 5.a, relative difference $|1-\eta_{sim}/\eta_{theo}|$, vs $|\eta_{theo}|$ from formula (III.15). Tilted curves: $y=10^{-6}/x$ and $y=10^{-6}x$

C. Peculiarities of the cylindrical PML

Figures 6 to 8 illustrate specific properties of the cylindrical geometry that have hardly any equivalent with Cartesian coordinates.

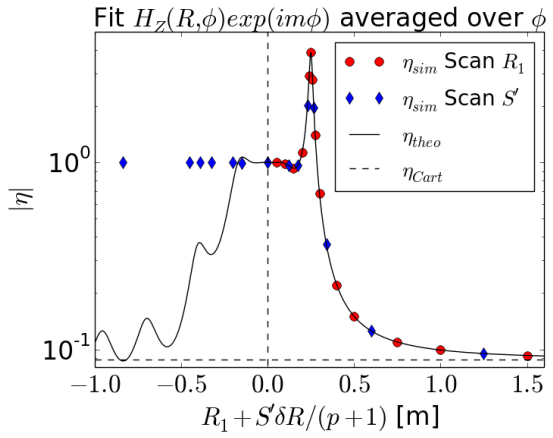

Figure 6: Simulated amplitude reflection coefficient $|\eta_{sim}|$ vs $Re(t_R(R_1))$. Numerical scan of R_1 with $S'=0$, scan of S' with $R_1=0.23$m and predictions $|\eta_{theo}|$ from formula (III.15). Horizontal dashed line: amplitude reflection coefficient $|\eta_{Cart}|$ from formula (III.17). Simulation series #8 and #9 from table 2.

Figure 6 shows a scan of the radial position R_1 for the inner PEC boundary of the simulation domain, with $S'=0$. Unlike expression $|\eta_{Cart}|$ from (III.17), the cylindrical reflection coefficient $|\eta_{theo}|$ from (III.15) depends on R_1. For given simulation parameters, a minimum value of R_1 exists below which the PML becomes inefficient. The variation of $|\eta_{sim}|$ with R_1 is non-monotonic. This corresponds to the crossing of peaks in the 2D diagrams on Figures 2. The maximal value of the reflection coefficient can exceed 1. For large R_1 the cylindrical curvature decreases at the PML location and $|\eta_{sim}|$ reaches an asymptotic value corresponding to $|\eta_{Cart}|$.

Figure 6 also shows that an effect similar to the change of R_1 is obtained by stretching the real part of R, through a scan of S' at fixed R_1. From formula (III.16) the relevant parameter to plot the results is $Re(t_R(R_1))=R_1+S'\delta R/(p+1)$. Negative values of this parameter can be reached, while R_1 remains positive. However Figure 6 shows that in these cases the PML fails to attenuate the incoming cylindrical wave, even when formula (III.15)

predicts low $|\eta_{theo}|$. This behavior may be linked with the crossing of a singular point of the coordinate system inside the PML. One should therefore avoid this parametric domain. The related simulation points were deliberately excluded from Figures 5.

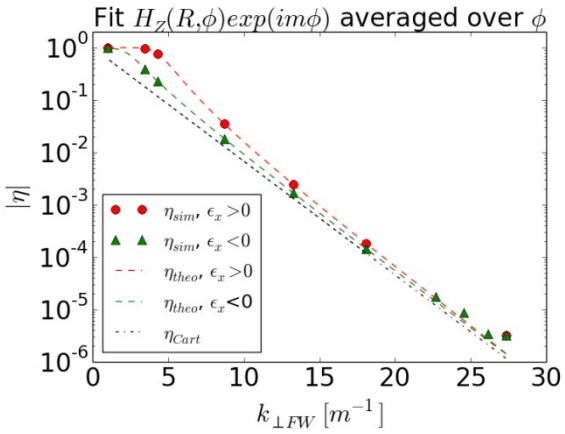

Figure 7: reflection coefficient over a scan of $\varepsilon_\times$, vs normal wavevector $k_{\perp FW}$ from equation (III.8). Data points with positive and negative $\varepsilon_\times$ are plotted with different symbols. Also shown are expressions $|\eta_{theo}|$ from formula (III.15) and $|\eta_{Cart}|$ from formula (III.17). Series #14 from table 2 with $\varepsilon_{//}$=-10^8

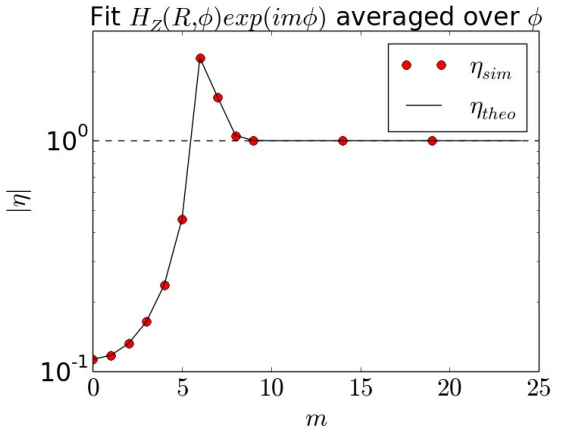

Figure 8: Numerical reflection coefficient η_{sim}, and prediction η_{theo} from formula (III-15) vs azimuthal mode number m. Simulation series #5 from table 2.

Figure 7 plots the simulated reflection coefficients *versus* wavevector $k_{\perp FW}$ from dispersion relation (III.8), over a scan of $\varepsilon_\times$ with $m\neq0$ (series #14 of Table 2). As for plane waves in Cartesian coordinates, low levels of reflection are observed for large $k_{\perp FW}$ while the PML loses efficiency for cylindrical waves propagating nearly parallel to the plasma/PML interface. However when $m\neq0$ cylindrical waves with positive and negative $\varepsilon_\times$ exhibit different $|\eta_{sim}|$ despite equal $k_{\perp FW}$. $|\eta_{sim}|$ values can differ by a factor of more than two. This specificity of the cylindrical geometry was anticipated from formula (III.15), where two terms appear in the numerator and denominator, one of which is proportional to $m\varepsilon_\times$. Largest ratios are obtained for medium values of $k_{\perp FW}$. For low $k_{\perp FW}$, $|\eta_{sim}|$ becomes 1 whatsoever. For large $k_{\perp FW}$ the reflection coefficients converge to $|\eta_{Cart}|$ from formula (III.17) that does not depend on the sign of $\varepsilon_\times$. In all cases $|\eta_{theo}|$ is larger than $|\eta_{Cart}|$. Figure 8 shows a scan of the azimuthal mode number m. Good agreement of $|\eta_{sim}|$ is found with $|\eta_{theo}|$ from formula (III.15). The variation of $|\eta_{sim}|$ with m is non-monotonic. This corresponds to the crossing of peaks in the 2D diagrams on Figures 2. The maximal value of the reflection coefficient can exceed 1. For large m, $|\eta_{sim}|$ reaches an asymptotic value of 1. A critical value of m is evidenced, above which the PML becomes inefficient.

V. Conclusions and prospects.

This paper formulated Perfectly Matched Layers (PMLs) for time-harmonic electromagnetic (EM) wave propagation in curved geometry. PMLs were obtained by artificially stretching a general set of three coordinates along complex trajectories. Major simplifications occurred since the original coordinate system was assumed orthogonal and we requested that the applied stretching preserve this orthogonality. Generalisation to coordinate systems with off-diagonal metric elements and/or non-orthogonal stretching presently appears more delicate. PMLs were defined as artificial lossy inhomogeneous materials that can be implemented in standard full-wave solvers for Maxwell's equations in the frequency-domain. In the adapted dielectric tensors and in the PML properties, not only the stretching functions

but also the stretched coordinates appear, accounting for the local curvature of the coordinate system. Specific formulae were given in cylindrical and toroidal geometries. Other sets of orthogonal coordinates could be treated similarly in the future, *e.g.* spherical coordinates for geophysical and astrophysical plasmas. Extension to transient EM pulse propagation would also be beneficial.

Stretching any system of coordinates does not necessarily ensure good PML properties in all cases. In cylindrical geometry the new formulation was assessed in a gyrotropic medium without losses, using an analytic reflection coefficient η_{theo} for propagative and evanescent cylindrical waves that play a role similar to the plane waves of Cartesian geometry. For simplicity this quantification was restricted here to radial PMLs and longitudinal anisotropy, in situations when only Transverse Electric modes of the medium play a role. PMLs in the longitudinal direction of our test problem behave like in Cartesian geometry. The exercise remains to be extended to PMLs in the azimuthal direction, azimuthal anisotropy, and/or more complex EM field polarizations, where incident and reflected waves from the two eigenmodes of the medium are coupled by the boundary conditions. The PML is expected to behave well if all the relevant eigenmodes are sufficiently attenuated before reaching the innermost boundary of the simulation domain. Indeed the boundary conditions only play a minor role in this situation. Analytical quantification of cylindrical TE wave reflection was complemented by finite-element simulations, showing better behaviour for the new PML formulation compared a Cartesian-like one artificially applied in cylindrical geometry.

In cylindrical geometry, like in Cartesian one, the proposed radial PML cannot be tuned to simultaneously attenuate forward and backward waves, a limitation inherent to our formulation. Reference [Bécache2017] explored ways to overcome this limitation, in uniaxial media and with Cartesian PMLs. As far as possible the radial extent δR of the PML should be large, at the expense of larger simulation domains. The PML behaves better for large wavevectors $k_\perp$ normal to the PML and exhibits limitations for cylindrical waves propagating nearly parallel to the plasma/PML interface. Combining the results for propagative and evanescent waves one can see that for given $k_\perp \delta R$, large positive values for S' and S'' provide a better behaviour for the radial PML. The counterpart is a larger radial variation of the dielectric properties of the adapted material. The PML region therefore requires finer radial discretization. Similar results were obtained in Cartesian geometry for S'' with propagative waves and for S' with evanescent waves [Jacquot2013].

Contrary to Cartesian PMLs, the real part of the radial coordinate stretch affects the reflection of propagative waves. This was interpreted as an artificial displacement of the radial location R_1 for the innermost PEC boundary towards regions of different cylindrical curvature. In practical applications, the geometry of the simulation domain often constrains the value of R_1. Stretching R_1 using S' can therefore be used to attenuate potential adverse effects of the local curvature, at the expense of refined mesh inside the PML. This method is also beneficial to better attenuate the evanescent waves, like in the Cartesian case. In numerical simulations, the PML loses efficiency when the real part of the stretched radius becomes negative. This behaviour was not predicted by the analytical figure of merit η_{theo}. This may be related with the crossing of a singular point of the coordinate system inside the PML domain.

For given plasma and fixed settings of the PML, a critical azimuthal mode number m always exists above which the PML loses efficiency. The critical m value can be made arbitrarily high by increasing the real or imaginary stretching, so that all m values relevant for a realistic simulation behave correctly. The associated numerical cost in terms of refined radial discretization depends on the requirements about the azimuthal resolution.

In reference [Jacquot2015] the new PML formulation was applied for the first time in realistic full-wave simulations of ion cyclotron wave propagation in the cold magnetized

plasma at the periphery of a tokamak. The geometry was a 2D radial-toroidal cut into the toroidal machine, in presence of toroidal curvature. It was described by cylindrical coordinates with azimuthal anisotropy of the plasma. The simulation domain was restricted to the vicinity of the wave launcher. Radial and azimuthal PMLs were applied at both the inner radial boundary and the two toroidal extremities of this domain.

Acknowledgements. Fruitful discussion with Pr. Bruno Després is gratefully acknowledged. This work has been carried out within the framework of the EUROfusion Consortium and has received funding from the Euratom research and training programme 2014-2018 under grant agreement No 633053. The views and opinions expressed herein do not necessarily reflect those of the European Commission.

VI. References

[Abramowitz]: M. Abramowitz & I. Stegun, « Handbook of mathematical functions », Dover publications.

[Angot1972]: A. Angot, "Compléments de mathématiques", 6th edition, Masson 1972 (in French)

[Bécache2017]: E. Bécache, P. Joly and M. Kachanovska, *Journal of Computational Physics* **341** (2017) pp. 76–101

[Bers1963]: W.P. Allis, S.J. Buchsbaum, A. Bers, "Waves in Anisotropic Plasmas", MIT press 1963, ch. 9 and 10 by A. Bers.

[Bilato2004]: R. Bilato et al., proc. 31st EPS Conference on Plasma Phys. London, 28 June - 2 July 2004 ECA Vol.28G, P-5.164 (2004),

[COMSOL]: https://www.comsol.com/

[Crombé2015]: Crombé, K. et al., *AIP Conference Proceedings*, **1689**, 030006 (2015)

[Ekedahl2015]: A. Ekedahl et al. AIP conf. Proc. **1689**, 030013-1 (2015)

[Faudot2015]: E. Faudot et al., *Review of Scientific Instruments*, **86** 063502 (2015).

[Furno2017]: I. Furno et al. *EPJ Web of Conferences* **157**, 03014 (2017) DOI: 10.1051/epjconf/201715703014

[Gedney1996]: Gedney et al. *IEEE trans. Ant. and Propag.* AP **44** p.1635 (1996)

[Gekelman2016]: W. Gekelman et al., *Rev. Sci. Instrum.* **87**, 025105 (2016).

[Goedbloed1981]: J.P. Goedbloed, *Computer Physics Communications* **24** (1981) pp. 311-321

[Goedbloed1982]: J.P. Goedbloed, *Physics of Fluids* **25**, p.2062 (1982)

[Gondarenko2004]: N. Gondarenko *et al.*, *Journal of Computational Physics* **194** (2004) pp. 481–504

[Jacquot2013]: J. Jacquot, et al., *PPCF* **55** (2013) 115004 (17pp)

[Jacquot2015]: J. Jacquot et al., *AIP Conference Proceedings* **1689**, 050008-1 050008-4 (2015)

[Louche2011]: F. Louche, P. Dumortier, A. Messiaen and F. Durodié, *Nucl. Fusion* **51** (2011) 103002 (20pp)

[Milanesio2017]: D. Milanesio et al. *EPJ Web of Conferences* **157**, 03034 (2017)

[Sachs1995]: Z.S. Sachs et al. *IEEE trans. Ant. and Propag.* AP **43** p.1460 (1995)

[Singer2004]: I. Singer, E. Turkel, "A perfectly matched layer for the Helmholtz equation in a semi-infinite strip", *Journal of Computational Physics* **201** (2004) pp.439–465

[Swanson2003]: D. Gary Swanson, "Plasma Waves" 2nd edition, IoP publishing, 2003

[Texeira1998]: F. L. Teixeira and W. C. Chew, IEEE Microwave and guided wave letters, vol. **8**, No. 6, JUNE 1998

[Velasco2009]: Mario Augusto Velasco Sanchez, “Improvements to a solver of the Helmholtz Equation », Master Thesis, Erasmus Mundus Program on Nuclear Fusion Science and Engineering Physics, Université Henri Poincaré, 2009